Intercalibration Between Special Sensor Microwave Imager/Sounder and Special Sensor Microwave Imager

Banghua Yan and Fuzhong Weng

***Abstract*—The F16 satellite was successfully launched on October 18, 2003, carrying the first Special Sensor Microwave Imager/Sounder (SSMIS) onboard. In this paper, the SSMIS imaging channels 12–18 are intercalibated against the F15 Special Sensor Microwave/Imager (SSM/I) instrument using Simultaneous Conical Overpassing (SCO) observations from both satellites. Results show that the SSMIS antenna temperatures have a mean bias as large as 1–2 K with a maximum of 3 K at 22.235 GHz with respect to F15. It appears that the mean biases at frequencies from 19.35 to 37 GHz do not strongly depend on the region and season, although the biases at the 91.655-GHz channels are slightly variable. The intercalibration analysis also shows that the nonlinearity may be one of the major sources resulting in differences between F15 SSM/I and F16 SSMIS measurements. For improved calibration and for the future SSM/I and SSMIS reprocessing, the SCO data are further utilized to resolve the SSMIS and SSM/I nonlinearity terms using a newly developed calibration algorithm. With the derived nonlinearity correction, the mean biases of the antenna temperatures between F15 and F16 are significantly reduced. To intercalibrate SSMIS to the same reference as SSM/I, SSMIS imaging channels can also be linearly mapped to the same and similar F15 SSM/I channels using the SCO matchup data. After the linear mapping, SSMIS snow-free land, snow, and sea ice surface emissivities are consistent with those derived from SSM/I.**

***Index Terms*—Intercalibration, nonlinearity, Simultaneous Conical Overpassing (SCO), Special Sensor Microwave/Imager (SSM/I), Special Sensor Microwave Imager/Sounder (SSMIS), surface emissivity.**

I. Introduction

ON October 18, 2003, the F16 satellite was successfully launched, carrying the Defense Meteorological Satellite Program (DMSP) Special Sensor Microwave Imager/Sounder (SSMIS) onboard. F16 SSMIS is the first operational microwave satellite radiometer for profiling temperature and humidity using a conical scanning mode, so that the viewing area and slant path remains nearly constant as it scans the Earth [1]. It has 24 channels to measure the Earth's radiation at frequencies between 19 and 183 GHz (see Table I). Among the 24 channels, the SSMIS offers seven window channels (channels 12–18) to continue the capability of DMSP Special Sensor Microwave/Imager (SSM/I) in monitoring and retrieving atmospheric and surface parameters such as precipitation, sea ice, ocean surface wind speed, columnar integrated liquid water, land surface temperature, emissivity, and soil moisture [2]–[6]. An excellent description of the SSMIS instrument has been given in [1]. After its launch, the SSMIS atmospheric sounding channels display persistent radiance anomalies. Several research groups are developing algorithms to detect and correct these anomalies in the sounding channels [7]–[14]. Since the radiance anomalies detected at the Lower Atmospheric Sounding (LAS) channels would tend to affect other channels, this paper investigates the quality of SSMIS window channel calibration through intersensor calibration.

This paper is organized as follows. In Section II, the SSMIS and SSM/I intercalibration methodology is described. In Section III, applications of the SSMIS and SSM/I intercalibration are given. Finally, the summary and conclusion are given in Section IV.

II. SSMIS and SSM/I Intercalibration Methodology

Recently, Cao *et al.* have developed a method to predict the time and location of the Simultaneous Nadir Overpasses (SNO) for the purpose of intercalibration among the different National Oceanic and Atmospheric Administration (NOAA) satellites [15]. Simultaneous observations between two satellites provide on-orbit monitoring of instrument performance through bias analysis and determination of instrument nonlinearity [15]–[17]. For two polar-orbiting satellites flying at different altitudes, an SNO event is found and an SNO data pair is generated when they cross an area at similar local times, where they observe the same Earth location at nadir nearly at the same time. A schematic viewing of the SNO event is shown in Fig. 1, where two satellites (NOAA 16 and NOAA 17) approach each other. For F15 and F16 satellites, the intercepting event happens once every few months, on average. Here, we modify the algorithms for SSMIS and SSM/I intersensor calibration because both instruments are conically scanning and have more

Manuscript received March 1, 2007; revised October 15, 2007. This work was supported by the Joint Center for Satellite Data Assimilation. The views expressed in this publication are those of the authors and do not necessarily represent those of NOAA.

B. Yan is with the Joint Center for Satellite Data Assimilation, National Oceanic and Atmospheric Administration, Camp Springs, MD 20746 USA, and also with Perot, Inc., Camp Springs, MD 20746 USA (e-mail: banghua.yan@noaa.gov).

F. Weng is with the Center for Satellite Applications and Research, National Oceanic and Atmospheric Administration, National Environmental Satellite Data and Information Service, Camp Springs, MD 20746 USA (e-mail: fuzhong.weng@noaa.gov).

Color versions of one or more of the figures in this paper are available online at http://ieeexplore.ieee.org.

Digital Object Identifier 10.1109/TGRS.2008.915752

0196-2892/$25.00 © 2008 IEEE

Authorized licensed use limited to: COLORADO STATE UNIVERSITY. Downloaded on July 30,2010 at 17:20:15 UTC from IEEE Xplore. Restrictions apply.

TABLE I
CHANNEL CHARACTERISTICS OF THE F16 SSMIS SENSOR [1]

Channel	Center Frequency (GHz)	3-db Width (MHz)	Frequency Stability (MHz)	Polarization	NEDT (K)	Sampling Interval (km)
1	50.3	380	10	V	0.34	37.5
2	52.8	389	10	V	0.32	37.5
3	53.596	380	10	V	0.33	37.5
4	54.4	383	10	V	0.33	37.5
5	55.5	391	10	V	0.34	37.5
6	57.29	330	10	RCP	0.41	37.5
7	59.4	239	10	RCP	0.40	37.5
8	150	1642(2)	200	H	0.89	12.5
9	183.31+/-6.6	1526(2)	200	H	0.97	12.5
10	183.31+/-3	1019(2)	200	H	0.67	12.5
11	183.31+/-1	513(2)	200	H	0.81	12.5
12	19.35	355	75	H	0.33	25
13	19.35	357	75	V	0.31	25
14	22.235	401	75	V	0.43	25
15	37	1616	75	H	0.25	25
16	37	1545	75	V	0.20	25
17	91.655	1418(2)	100	V	0.33	12.5
18	91.655	1411(2)	100	H	0.32	12.5
19	63.283248+/-0.285271	1.35(2)	0.08	RCP	2.7	75
20	60.792668+/-0.357892	1.35(2)	0.08	RCP	2.7	75
21	60.792668+/-0.357892+/-0.002	1.3(4)	0.08	RCP	1.9	75
22	60.792668+/-0.357892+/-0.0055	2.6(4)	0.12	RCP	1.3	75
23	60.792668+/-0.357892+/-0.016	7.35(4)	0.34	RCP	0.8	75
24	60.792668+/-0.357892+/-0.050	26.5(4)	0.84	RCP	0.9	37.5
Notes	(1) Sampling refers to along scan direction based on 833km spacecraft altitude. (2) NEDT for instrument temperature 0°C and calibration target 260K with integration times of 8.4 msec for Channels 12-16; 12.6 msec for Channels 1-7, 24; and 25.2 msec for Channels 19-23 and 4.2 msec for Channels 8-11, 17-18. (3) Number of sub-bands is indicated by (n) next to individual 3-db width (4) RCP denotes right-hand circular polarization.					

chances for matching up in space and time. This is called Simultaneous Conical Overpass (SCO).

The frequency of occurrence of SNO (or SCO) events depends on the criteria of simultaneity. Although SNO (or SCO) events occurring within a few seconds or less regularly occur for succeeding satellites [16], the number of nadir (or fixed angle) viewing samples can be small depending on the temporal range and spatial distance criteria. In this paper, the SCO constraints on temporal and spatial windows are relaxed to have more matchup data, considering that the precise matching

Authorized licensed use limited to: COLORADO STATE UNIVERSITY. Downloaded on July 30,2010 at 17:20:15 UTC from IEEE Xplore. Restrictions apply.

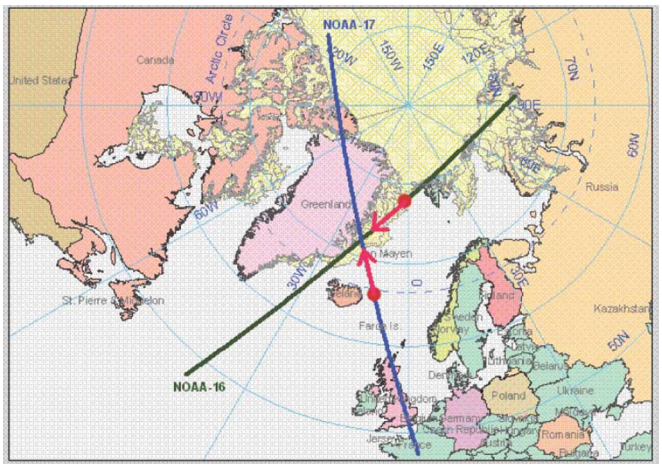

Fig. 1. Schematic viewing the overpasses between two satellites [15].

events mainly occur in high latitudes where surface and atmosphere are relatively stable. The distance window from two sensors is set to a ground distance of 12.5 km, and the time window is set to 60 s. Our analyses are based on all the SCO events between F15 SSM/I and F16 SSMIS because they are both the midmorning satellites and cross an area at similar local times. Fig. 2 shows the most SCO event distributions between SSM/I instruments. The SCO distributions between F15 and F16 are similar to them. It is found that the SCOs regularly occur in the latitude between 70° and 80°.

There remain some differences in the F15 and 16 SCO observations due to their spatial and temporal mismatches. The 22.235-GHz channel is sensitive to water vapor, whereas the 37- and 91.655-GHz channels are significantly affected by cloud liquid water. Currently, the SCO observations may include samples under cloudy conditions due to lack of cloud-screening algorithms over various surfaces. According to our sensitivity test, brightness temperatures at 22.235 and 37 GHz vary within 0.2 and 0.5 K, respectively, for a cloud liquid water path ranging from 0 to 0.3 mm. Thus, the effect of clouds on satellite microwave measurements at lower frequencies in polar areas is relatively small. However, due to their large field of views (FOVs) at low frequencies, satellite measurements near two surface boundaries (e.g., sea ice and water) may display large contrasts [5]. In addition, the SCO observations are also not quality controlled through the azimuthal angle. Our quality control is based on [18], which checked the surface inhomogeneity using their SCO standard deviation. When the SCO samples near a location from each satellite produce a standard deviation larger than 1 K, the whole samples are rejected from the intercalibration. After the quality control, the SCO observations between F16 and F15 are more than 5000 occurrences over both Arctic and Antarctic areas (see Table II).

A. Bias Characteristics of SSMIS Antenna Temperatures

Fig. 3(a)–(g) displays the F16 and F15 antenna temperatures at channels from 19.35 to 91.655 GHz from the SCO observations. SCO observations are obtained from January 1, 2005, to August 13, 2006. We stopped the data after August 13 because there is a significant radar calibration beacon interference in

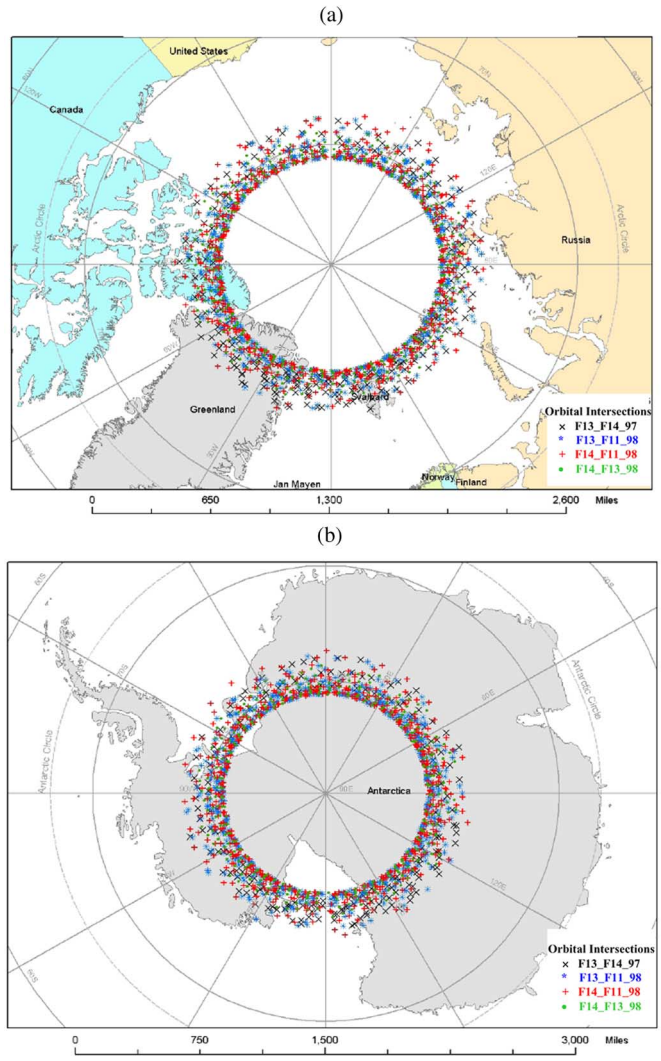

Fig. 2. SCO event distributions for SSM/I instruments over (a) Orbital Intersections near the Arctic between DMSP satellites and (b) Orbital Intersections near the Antarctica between DMSP satellites.

TABLE II
F16 SSMIS ANTENNA TEMPERATURE MEAN BIASES AND STANDARD DEVIATIONS IN CONTRAST TO F15 SSM/I DATA AT THE SEVEN WINDOW CHANNELS OVER THE ARCTIC, ANTARCTIC, AND CLOUD-FREE OPEN OCEANS

Frequency (GHz)	Arctic SCO samples: 5901		Antarctic SCO samples: 9540		Cloud-Free Samples>100, 000	
	Mean Bias	Standard Deviation	Mean Bias	Standard Deviation	Mean Bias	Standard Deviation
19.35 (V)	0.9	0.8	1.2	0.8	1.4	2.0
19.35 (H)	-0.3	0.6	0.0	0.6	0.2	3.6
22.235 (V)	3.2	1.6	3.7	1.6	3.6	3.5
37 (V)	2.7	1.1	2.8	1.0	3.0	1.9
37 (H)	0.6	1.4	0.4	1.4	1.0	3.9
91.655 (V)	-0.2	1.4	-0.2	1.3	-0.1	2.4
91.665 (H)	-0.1	1.6	-0.1	1.6	0.6	4.0

F15 22.235 GHz [19], [20]. The SCO collocations from the ten beam positions near the scan edges are not used in this paper due to possible intrusions by the Glare Suppression

Authorized licensed use limited to: COLORADO STATE UNIVERSITY. Downloaded on July 30,2010 at 17:20:15 UTC from IEEE Xplore. Restrictions apply.

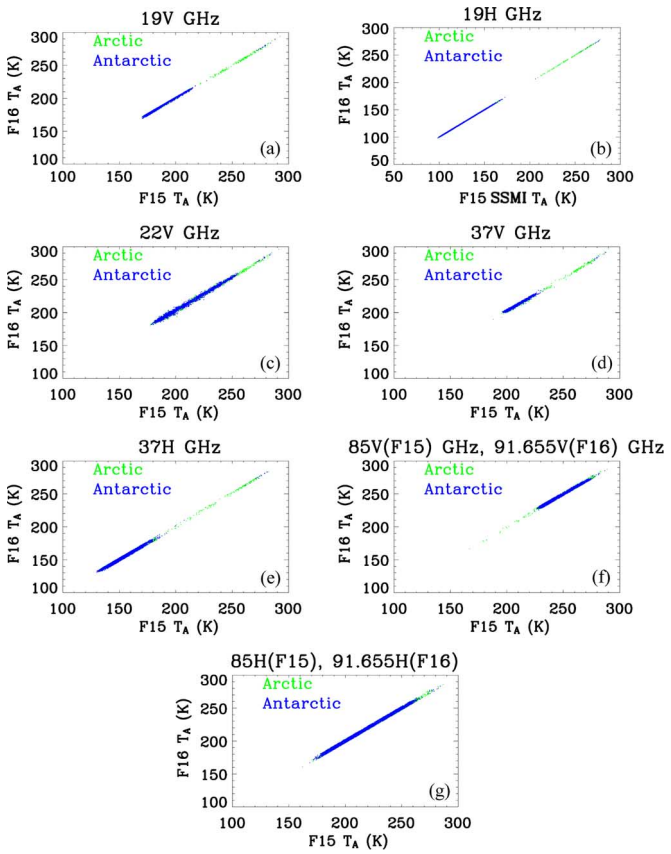

Fig. 3. SSMIS antenna temperatures against F15 SSM/I antenna temperatures based on the SCO observations during the period from January 1, 2005, to August 13, 2006, where the green color denotes the results over Arctic, whereas the blue color denotes the results over Antarctic. (a) 19.25 GHz for V-POL. (b) 19.35 GHz for H-POL. (c) 22.235 GHz for V-POL. (d) 37 GHz for V-POL. (e) 37 GHz for H-POL. (f) 85 (91.655) GHz for V-POL. (g) 85 (91.655) GHz for H-POL.

System-B [19], [21]. The mean biases of the SSMIS antenna temperatures from F15 SSM/I data are also shown. Overall, F16 antenna temperature biases occur at most of the channels, and the maximum bias of about 3.7 K occurs at 22.235 GHz. Note that the mean bias at high latitudes over the Arctic is usually different from that over the Antarctic. For example, at 19.35 GHz, the mean biases are 0.9 and 1.2 K, respectively, for the Arctic and Antarctic. Table II is a summary including the sample number of SCO observations, mean biases, and standard deviations of the SSMIS antenna temperature biases at the seven channels over the Arctic and Antarctic.

These antenna temperature biases and/or their differences over the Arctic and Antarctic may result from the differences in the instrument configurations, which include the following: 1) Earth incidence angle (EIA); 2) antenna pattern; 3) anomaly associated with calibration targets and reflector; and 4) nonlinear term in the calibration equation. At 91.655 GHz, SSMIS antenna temperatures are compared with SSM/I measurements at 85.5 GHz, where the biases are also affected by the frequency shift, in which the emission and scattering from atmosphere and surface may slightly differ. The following discussions will primarily focus on the error sources from 1) to 3), whereas the nonlinear term will be discussed in Section II-B.

TABLE III
F15 AND F16 SSM/I APF-RELATED COEFFICIENTS, IN WHICH THE F16 AP AND BP COEFFICIENTS ARE PROVIDED BY S. SWADLEY (PERSONAL COMMUNICATION)

Frequency (GHz)	AP		BP	
	F15 SSM/I	F16 SSMIS	F15 SSM/I	F16 SSMIS
19V	0.9690	0.9720	0.00473	0.00441
19H	0.9690	0.9680	0.00415	0.00503
22V	0.9740	0.9820	0.01070	0.00292
37V	0.9860	0.9850	0.02170	0.00415
37H	0.9860	0.9810	0.02612	0.00343
85V (92V)	0.9880	0.9820	0.01383	0.01319
85H (92H)	0.9880	0.9780	0.01947	0.01876

For F15 SSM/I and F16 SSMIS, their EIAs are approximately 53.1° when the instruments were launched [1], [22]. The satellite altitude change may result in slight changes in the EIA. However, simulations using our radiative transfer model show that the change of antenna temperatures is small when the EIA varies in a small range. For instance, the mean changes in antenna temperatures at the seven channels over land are usually smaller than 0.2 K for about a 1° change in the EIA. Thus, the EIA change is not a main contributor to the bias. However, the antenna pattern function (APF) for F15 and F16 is not necessarily the same, thus affecting the bias between the two instruments. This can be roughly detected by calculating the brightness temperature difference using F16 APF coefficients for F15 temperature data record (TDR) calculations. The antenna pattern correction procedure [21] was used to convert the F15 antenna temperatures T_A to brightness temperatures T_B such as

$$T_{B,V} = \frac{1}{\mathrm{AP}_V(1-\mathrm{BP}_V)}T_{A,V} - \frac{\mathrm{BP}_V}{\mathrm{AP}_V(1-\mathrm{BP}_V)}T_{A,H} \quad (1)$$

$$T_{B,H} = \frac{1}{\mathrm{AP}_H(1-\mathrm{BP}_H)}T_{A,H} - \frac{\mathrm{BP}_H}{\mathrm{AP}_H(1-\mathrm{BP}_H)}T_{A,V} \quad (2)$$

where the coefficients AP and BP are given in Table III for both satellites, and the subscripts "V" and "H" represent V-POL and H-POL, respectively. By using (1) and (2), the antenna temperature difference between two satellites can be thus derived from their brightness temperature difference, or vice versa. It is shown in Table IV that the mean antenna temperature differences at frequencies from 19.35 to 37 GHz vary from −1.99 to 1.6 K in polar areas. The results at 91.655-GHz channels are not shown in this table because the departure of the SSMIS 91.655-GHz channels also contains the frequency dependence. Thus, the antenna pattern difference has some major impacts on the antenna temperature discrepancies.

The F16 antenna temperatures at its LAS channels exhibited anomalies as large as 2 K due to thermal emission of the main reflector (so-called antenna emission) and solar radiation impinging on warm counts at the LAS channels [11]–[14].

Authorized licensed use limited to: COLORADO STATE UNIVERSITY. Downloaded on July 30,2010 at 17:20:15 UTC from IEEE Xplore. Restrictions apply.

TABLE IV
F16 ANTENNA TEMPERATURE BIASES WITH RESPECT TO F15 ($\Delta T_A^{\mathrm{APF}}$) AT FREQUENCIES FROM 19.35 TO 37 GHz, RESULTING FROM THE APF DIFFERENCES BETWEEN F15 AND F16

Frequency (GHz)	$\Delta T_A^{\mathrm{APF}}$(K)
19.35 (V)	-0.72
19.35 (H)	0.17
22.235 (V)	-1.99
37 (V)	-0.18
37 (H)	1.60

Those anomalies are also strongly dependent on the season and region. For example, the anomaly resulting from the antenna emission can reach a maximum of about 2 K at high latitudes but reduces to about 0.5 K at low and middle latitudes [14]. The antenna emission detected at the LAS channels may be also manifested at other channels and must be assessed for improved calibration. For a sanity check, we have extended our collocated data between F15 and F16 satellites over oceans under cloud-free atmospheres between 60°N and 60°S. In this process, a time difference less than 10 min is utilized, and the cloud-contaminated observations are identified by using the cloud liquid water algorithm [2]. Note that the so-collocated data are distinctive from the aforementioned SCO observations due to their much larger time difference. To reduce the influences due to variable atmospheric and surface properties, the collocated data are generated throughout 2005. The yearly mean SSMIS antenna temperature biases and standard deviations at the seven window channels are also shown in Table II. Overall, the mean SSMIS antenna temperature biases in polar areas are basically consistent with those over oceans, generally smaller than 0.5 K. An increased antenna temperature bias at SSMIS H-POL 91.655 GHz is partially due to the frequency shift to SSM/I 85 GHz. This feature agrees with our simulations, in which the H-POL brightness temperature at 91.655 GHz is usually warmer than that at 85 GHz. The longitudinal mean biases of F16 antenna temperatures at the seven imaging channels, the standard deviations of the biases, and their time series in 2005 are further analyzed based on the aforementioned collocated data over cloud-free open oceans as follows.

Fig. 4(a)–(g) displays the longitudinal mean biases of F16 antenna temperatures and the corresponding standard deviations at the seven channels, whereas Fig. 4(h) displays the sample number versus latitude. The biases at the V-POL 19.35- and 37-GHz channels are relatively stable throughout all latitudes, whereas those at H-POL 19.35- and 22.235-GHz channels exhibit some variations. These increased variations are primarily caused by the increasing effects of atmospheres, which have more variability. Overall, the mean biases between two satellites over oceans are consistent with those using the SCO matchup data set over polar areas with a difference less than 0.5 K. Therefore, the F16 antenna temperature biases at these five window channels are small and within the SSMIS noise levels.

At 91.655 GHz, the F16 biases to F15 exhibit large variations for latitudes within 40°. These variations may be related to the increased effects from the cloud water path at higher frequencies. In addition, they are possibly related to the antenna emission. According to the theoretical simulations, the emissivity of the F16 main reflector increases with frequency [7]. This would produce an antenna emission higher than 2 K, which has been confirmed in SSMIS LAS channels. Separation of the causes of biases from the aforementioned effects (i.e., atmospheric emission and antenna emission) would require our further knowledge. This is because there is a further complication in diagnosing the antenna emission for different groups of channels. The F16 SSMIS window channel biases are referred to the F15 satellite, whereas the SSMIS sounding channel biases are defined to the simulated channels with numerical weather prediction fields. The different calibration references may result in some inconsistencies in bias properties. Thus, more studies are needed to understand the root cause of the antenna temperature biases at the 91.655-GHz channels.

Fig. 5(a)–(g) further displays the monthly mean biases of F16 antenna temperatures and the corresponding standard deviations for 11 months of 2005. The sample number of the collocated data for each month is larger than 30 000. It is found that the monthly mean biases at the lower frequency channels from 19.35 to 37 GHz do not exhibit a pronounced seasonal variation.

Overall, the characteristics of F16 antenna temperature mean biases at frequencies from 19.35 to 37 GHz are similar over different regions and seasons, indicating that the antenna emission detected at the LAS channels is insignificant at these window channels. These biases may be attributed to a lack of nonlinearity correction in calibration and inaccurate correction of the antenna spillover and cross-polarization effects. For the 91.655-GHz channels, the mean biases of F16 antenna temperatures display slightly larger variations with the latitude and season.

B. Nonlinearity in the SSMIS and SSM/I Calibration

The antenna temperature T_A, including the nonlinearity term, is given as follows [14], [25]:

$$T_A = T_{AL} + \mu Z \tag{3}$$

where

$$T_{AL} = T_C + S(C_S - C_C),$$
$$Z = S^2(C_S - C_C)(C_S - C_W),$$
$$S = \frac{T_W - T_C}{C_W - C_C}.$$

Here, C_S, C_C, and C_W denote the counts of Earth scene, cold space, and warm target, respectively; μ is the nonlinear parameter. Also, T_C is the deep-space cosmic background temperature, and T_W is the brightness temperature of the warm target, which is determined by the physical temperature (the warm target emissivity is considered close to unity) measured using platinum resistance thermistors.

Authorized licensed use limited to: COLORADO STATE UNIVERSITY. Downloaded on July 30,2010 at 17:20:15 UTC from IEEE Xplore. Restrictions apply.

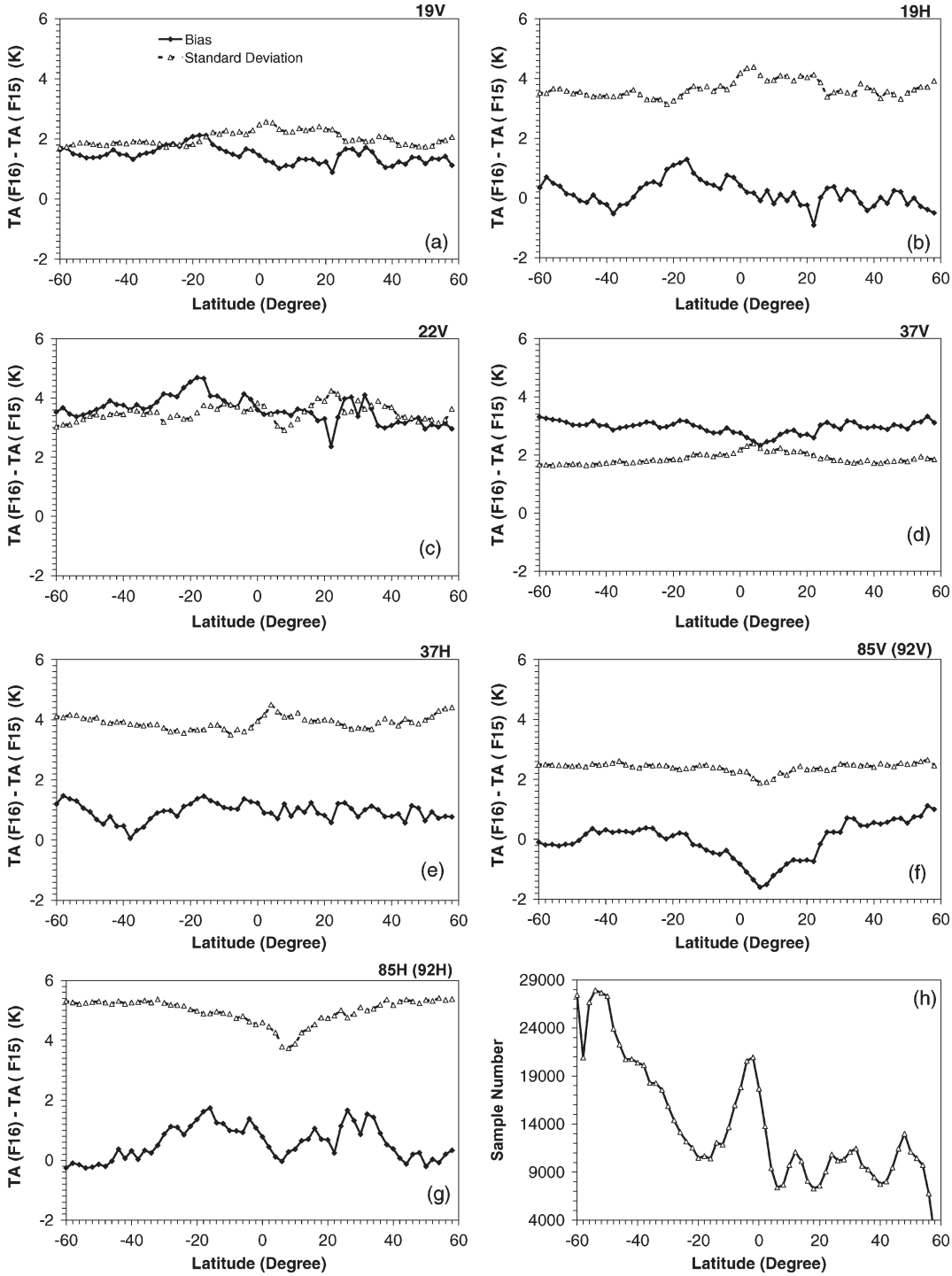

Fig. 4. Longitudinal mean biases of F16 antenna temperatures and corresponding standard deviations against latitude with respect to F15 measurements, which are calculated using the matchup data between F15 and F16 over cloud-free open oceans between 60°N and 60°S. (a) 19.25 GHz for V-POL. (b) 19.35 GHz for H-POL. (c) 22.235 GHz for V-POL. (d) 37 GHz for V-POL. (e) 37 GHz for H-POL. (f) 85 (91.655) GHz for V-POL. (g) 85 (91.655) GHz for H-POL. (h) Sample number versus latitude. The legends used in (a) are also applicable for (b)–(g).

The nonlinearity term defined by μZ is proportional to the radiometric counts from an Earth-viewing scene and is thus dependent on the corresponding antenna temperature. As analyzed in Section II, the antenna temperature biases are still obvious at most of the window channels, although all other error sources are accounted for. Thus, it is necessary to quantify the nonlinearity term for either F15 or F16. Zou *et al.* developed an algorithm to derive the nonlinear parameters for Microwave Sounding Unit (MSU) instruments using the prelaunch nonlinear parameter of one reference satellite [17]. In the SSM/I and SSMIS calibration, however, the nonlinear parameters were not available from their prelaunch analysis.

Therefore, a new algorithm is developed for determining this parameter from the SCO observations over the Arctic

Authorized licensed use limited to: COLORADO STATE UNIVERSITY. Downloaded on July 30,2010 at 17:20:15 UTC from IEEE Xplore. Restrictions apply.

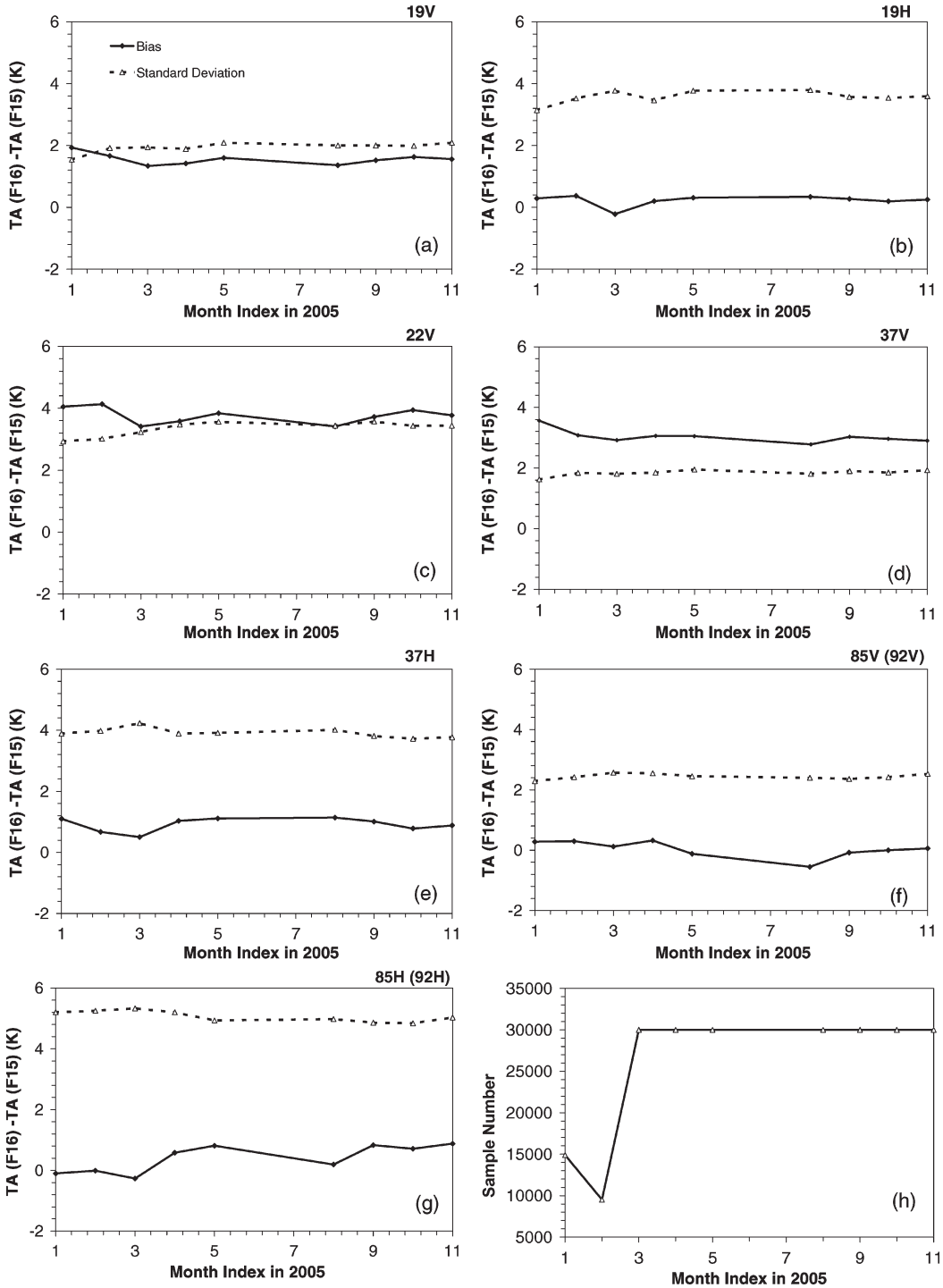

Fig. 5. Monthly mean biases of F16 antenna temperatures and corresponding standard deviations against month with respect to F15 measurements, which are calculated using the matchup data between F15 and F16 over cloud-free open oceans between 60°N and 60°S. (a) 19.25 GHz for V-POL. (b) 19.35 GHz for H-POL. (c) 22.235 GHz for V-POL. (d) 37 GHz for V-POL. (e) 37 GHz for H-POL. (f) 85 (91.655) GHz for V-POL. (g) 85 (91.655) GHz for H-POL. The legends used in (a) are also applicable for (b)–(g).

and Antarctic, which does not rely on the assumption of any reference satellites, as described in the following.

Applying (3) to satellites K and J results in

$$T_{A,K} = T_{\mathrm{AL},K} + \mu_K Z_K \tag{4}$$

$$T_{A,J} = T_{\mathrm{AL},J} + \mu_J Z_J \tag{5}$$

where μ_J and μ_K denote the nonlinear parameters for satellites J and K, respectively.

Then, the difference between $T_{A,K}$ and $T_{A,J}$, i.e., ΔT, can be expressed as

$$\Delta T = (T_{\mathrm{AL},K} - T_{\mathrm{AL},J}) + (\mu_K Z_K - \mu_J Z_J) \tag{6}$$

Authorized licensed use limited to: COLORADO STATE UNIVERSITY. Downloaded on July 30,2010 at 17:20:15 UTC from IEEE Xplore. Restrictions apply.

TABLE V
NONLINEAR PARAMETERS (μ) AT FREQUENCIES FROM 19.35 TO 37 GHz FOR F15 AND F16 INSTRUMENTS

Frequency (GHz)	Nonlinear Parameter (μ)	
	F15	F16
19.35 (V)	-7.0449E-6	1.0913E-5
19.35 (H)	-1.1059E-6	-1.0825E-6
22.235 (V)	-5.4371E-5	6.7848E-5
37 (V)	-5.6897E-5	7.1057E-5
37 (H)	-1.7801E-5	2.2946E-5

or

$$\Delta T = \Delta T_{\mathrm{AL}} + (\mu_K Z_K - \mu_J Z_J) \tag{7}$$

where $\Delta T_{\mathrm{AL}} = T_{\mathrm{AL},K} - T_{\mathrm{AL},J}$.

For two sensors when they observed the same locations (i.e., their SCO observations), $\Delta T = 0$, i.e.,

$$\Delta T_{\mathrm{AL}}(K, J) + (\mu_K Z_K - \mu_J Z_J) = 0. \tag{8}$$

The differential surface properties between the Arctic and Antarctic usually result in a difference in $\Delta T_{\mathrm{AL}}(K, J)$ and Z_K. Therefore, we derive a set of equations, i.e.,

$$\Delta T_{\mathrm{AL}}^{\mathrm{Arctic}} + (\mu_K Z_K^{\mathrm{Arctic}} - \mu_J Z_J^{\mathrm{Arctic}}) = 0 \tag{9}$$

$$\Delta T_{\mathrm{AL}}^{\mathrm{Antarctic}} + (\mu_K Z_K^{\mathrm{Antarctic}} - \mu_J Z_J^{\mathrm{Antarctic}}) = 0. \tag{10}$$

With algebraic operation, we obtain

$$\mu_K = \frac{\Delta T_{\mathrm{AL}}^{\mathrm{Arctic}}/Z_J^{\mathrm{Arctic}} - \Delta T_{\mathrm{AL}}^{\mathrm{Antarctic}}/Z_J^{\mathrm{Antarctic}}}{Z_K^{\mathrm{Arctic}}/Z_J^{\mathrm{Arctic}} - Z_K^{\mathrm{Antarctic}}/Z_J^{\mathrm{Antarctic}}} \tag{11}$$

$$\mu_J = \frac{\Delta T_{\mathrm{AL}}^{\mathrm{Arctic}}}{Z_J^{\mathrm{Arctic}}} + \frac{Z_K^{\mathrm{Arctic}}}{Z_J^{\mathrm{Arctic}}}\mu_K. \tag{12}$$

Equations (11) and (12) may be ill-posed when the denominator in (11) is very small. In these circumstances, the nonlinearity term cannot be resolved. Thus, when the denominator in (11), i.e., $(Z_K^{\mathrm{Arctic}}/Z_J^{\mathrm{Arctic}}) - (Z_K^{\mathrm{Antarctic}}/Z_J^{\mathrm{Antarctic}}) < 0.15$, we do not compute this parameter. By setting this quality control, the mean nonlinear parameters for F15 and F16 instruments are derived by solving (11) and (12) from their SCO observations. Note that $\Delta T_{\mathrm{AL}}^{\mathrm{Arctic}}$ and $\Delta T_{\mathrm{AL}}^{\mathrm{Antarctic}}$ in (11) and (12) have removed the effect of the antenna pattern difference based on Table IV. Table V displays the nonlinear parameters of F15 and F16 at five channels from 19.35 to 37 GHz. Since the departure of the SSMIS 91.655-GHz channels also contains the frequency dependence, their nonlinear parameters are not studied here.

According to those nonlinear parameters, the nonlinearity term in (3) for F15 and F16 can be estimated. Fig. 6(a)–(e) displays the nonlinearity at frequencies from 19.35 to 37 GHz computed using the newly derived nonlinear parameters. One sees that the nonlinearities (absolute value) at V-POL 22.235 and 37 GHz are relatively large and reach to about 1 K, whereas the nonlinearity at H-POL 19.35 GHz is the least (usually smaller than 0.3 K). This conclusion is consistent with the aforementioned SSMIS observation biases because the bigger the observation differences, the larger the nonlinearity, according to (11). In addition, with those nonlinear parameters, the antenna temperatures from 19.35 to 37 GHz for F15 and F16 instruments can be recalibrated using the nonlinear calibration (3). Fig. 7(a)–(e) shows the time series of the linear and nonlinear calibrated SSMIS antenna temperature biases from 19.35 to 37 GHz, which are calculated from the linear calibration equation, i.e., ignoring the second term on the right side in (3), and the nonlinear calibration equation using (3), respectively. Note that the bias caused by the APF difference has been removed from Fig. 7. One obvious feature is observed from the figures: the SSMIS antenna temperature biases are significantly reduced, and the mean bias is usually smaller than 0.3, as the nonlinear calibration is applied into both F15 and F16 observations. Therefore, the mean bias of antenna temperatures between the F15 and F16 satellites may be reduced through nonlinearity correction. Those preliminary results demonstrated that the nonlinearity seems to be nonnegligible in future SSM/I and SSMIS reprocessing. Fig. 7(f) displays the residual V-POL/H-POL SSMIS antenna temperature errors at frequencies from 19.35 to 37 GHz, after the nonlinear calibration is applied to both F15 and F16 observation. It is found that the residual bias (mean) is usually within ± 0.3 K, except for V-POL 22.235-GHz, where the absolute bias is around 0.4 K. Moreover, there remains a certain difference in biases over the Arctic and Antarctic regions at some channels.

C. SSMIS Remapping to SSM/I Observations

In the SSMIS calibration, we also tested direct linear mapping between SSMIS imaging channels and SSM/I using

$$T'_{A,\mathrm{ich}} = \alpha_{\mathrm{ich}} + \beta_{\mathrm{ich}} T_{A,\mathrm{ich}} \tag{13}$$

where α_{ich} and β_{ich} denote the offset and slope, respectively, and both of them are produced by using SCO observations between SSMIS and SSM/I; the subscript "ich" is the SSMIS channel corresponding to each of the seven SSMI-like channels, i.e., $i = 12,\ 11,\ 13,\ 15,\ 14,\ 18,$ and 17. Table VI displays the derived offset and slope values. Note that those remapping coefficients are derived from linear calibrated F15 and F16 observations. This is because all SSM/I and SSMIS observations used in the public community are currently calibrated using the linear calibration equation. Therefore, (13) provided an efficient conversion between SSMIS and SSM/I, where F15 SSM/I observations are set as a reference. Note that this process also makes SSMIS 91.655 GHz as SSM/I 85 GHz.

III. APPLICATIONS OF THE SSMIS AND SSM/I INTERCALIBRATION

Under clear skies, the satellite observation (T_B) can be reliably simulated using an emission-based radiative transfer equation [2], as follows:

$$T_B = \varepsilon T_s \zeta + T_u + (1 - \varepsilon) T_d \zeta \tag{14}$$

Authorized licensed use limited to: COLORADO STATE UNIVERSITY. Downloaded on July 30,2010 at 17:20:15 UTC from IEEE Xplore. Restrictions apply.

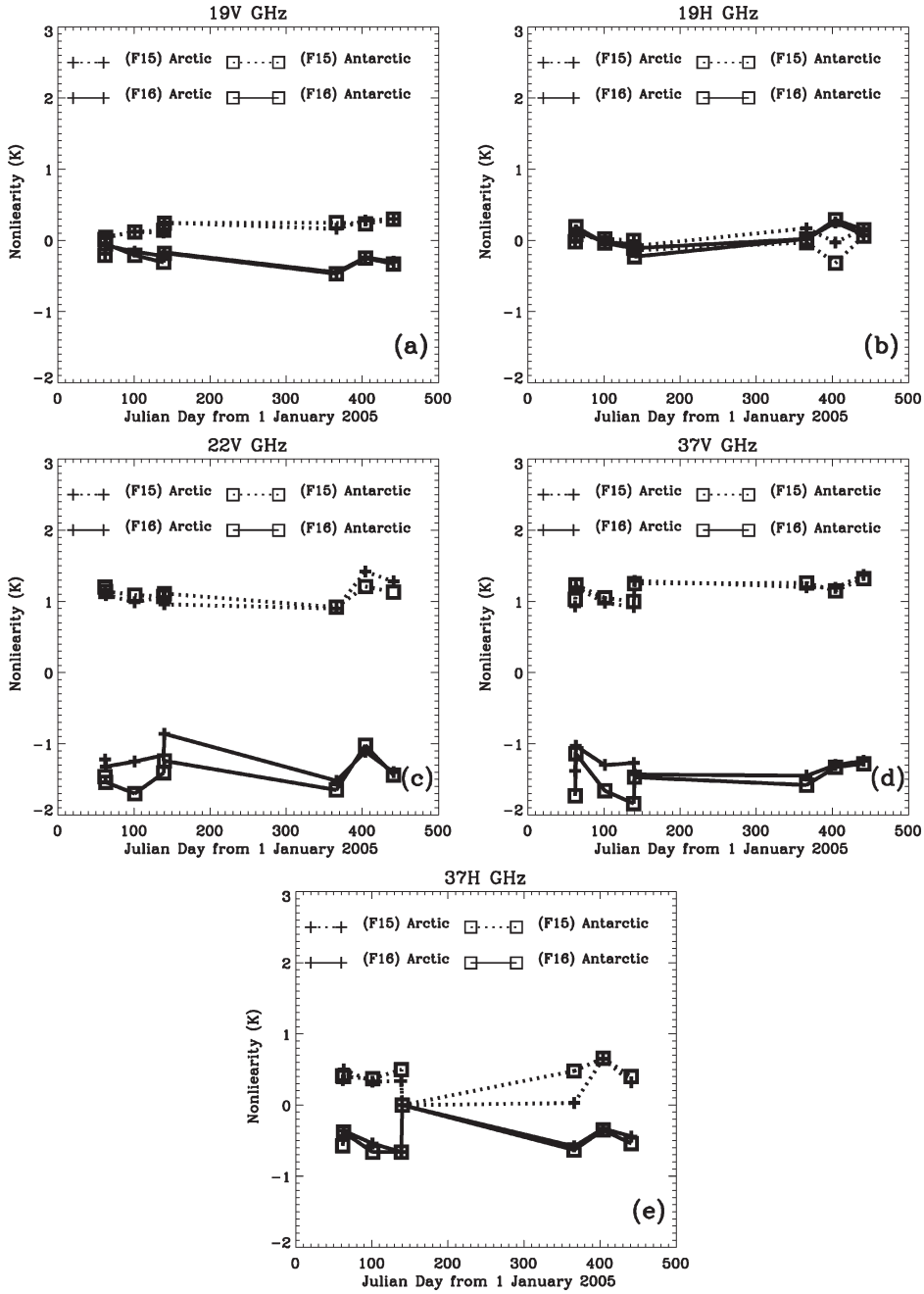

Fig. 6. Time series of nonlinearities of F15 and F16 instruments at frequencies from 19.35 to 37 GHz over the Arctic and Antarctic computed using the newly derived nonlinear parameters. (a) V-POL 19.35 GHz. (b) H-POL 19.35 GHz. (c) V-POL 22.235 GHz. (d) V-POL 37 GHz. (e) H-POL 37 GHz.

with

$$\zeta = e^{-\tau/\cos(\theta)}$$

$$T_d = \int_0^{\tau} T(\tau') e^{-(\tau-\tau')/\cos(\theta)} d\tau'/\cos(\theta)$$

$$T_u = \int_0^{\tau} T(\tau') e^{-\tau'/\cos(\theta)} d\tau'/\cos(\theta)$$

where θ is the local zenith angle, ε is the surface emissivity, T_s is the surface temperature, τ is the optical depth, ζ is the atmospheric transmittance, and T_u and T_d are the brightness temperatures associated with upwelling and downwelling radiation, respectively. All of ζ, T_u, and T_d can be obtained from the absorption model for the given atmospheric profiles of temperature and water vapor, such as National Centers for Environmental Prediction Global Data Assimilation System analysis products. Thus, emissivity can be computed using (14) in the clear skies.

Notice that T_B in (14) is the brightness temperature, i.e., the remapped antenna temperature from (13) needs to do antenna spillover and cross-polarization corrections. Since those corrections are related to some nonlinear (scattering) processes at a specific frequency and polarization over some surfaces, the brightness temperature spectrum may be different from the antenna temperature spectrum for a specific surface. Fig. 8(a)–(d) displays the V-POL antenna and brightness temperature spectra

Authorized licensed use limited to: COLORADO STATE UNIVERSITY. Downloaded on July 30,2010 at 17:20:15 UTC from IEEE Xplore. Restrictions apply.

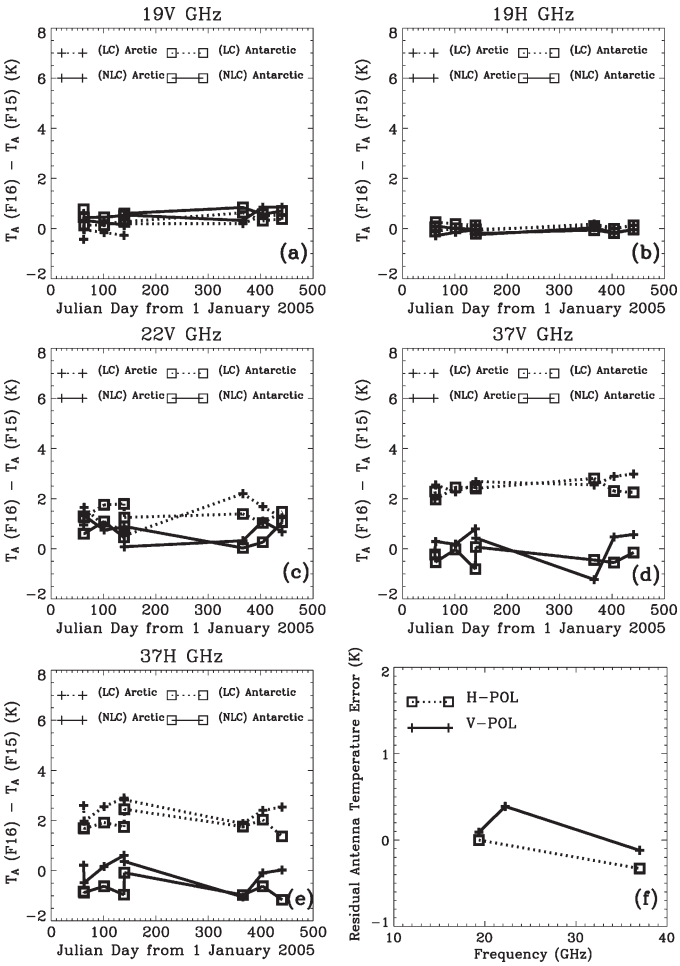

Fig. 7. Time series of F16 antenna temperature biases at frequencies from 19.35 to 37 GHz over the Arctic and Antarctic, which are computed using linear and nonlinear calibration equations, respectively. In the figure, "LC" denotes linear calibration, whereas "NLC" denotes nonlinear calibration. (a) V-POL 19.35 GHz. (b) H-POL 19.35 GHz. (c) V-POL 22.235 GHz. (d) V-POL 37 GHz. (e) H-POL 37 GHz. (f) Residual antenna temperature difference at V/H-POL, after the nonlinear calibration is applied to both F15 and F16 observations.

TABLE VI
OFFSET AND SLOPE VALUES USED FOR LINEARLY REMAPPING THE F16 SSMIS ANTENNA TEMPERATURE AT THE SEVEN SSM/I-LIKE CHANNELS TO F15 SSM/I ANTENNA TEMPERATURES

Frequency (GHz)	α	β
19.35 (V)	-2.03627	1.00623
19.35 (H)	0.00424	1.00027
22.235 (V)	-2.52875	0.99642
37 (V)	-3.86053	1.00550
37 (H)	0.80170	0.99139
91.655 (V)	-7.43913	1.03121
91.655 (H)	1.53650	0.99317

over four typical surfaces (e.g., snows, desert, canopy, and bare soil), respectively. A stronger frequency dependence is detected in the brightness temperature spectrum than in the antenna temperature spectrum, particularly over nonsnow surfaces. A similar conclusion is obtained from the H-POL antenna and brightness temperature spectra (figures are omitted). Thus, the use of antenna temperatures for emissivity simulations could cause some misleading discussions for the surface emissivity

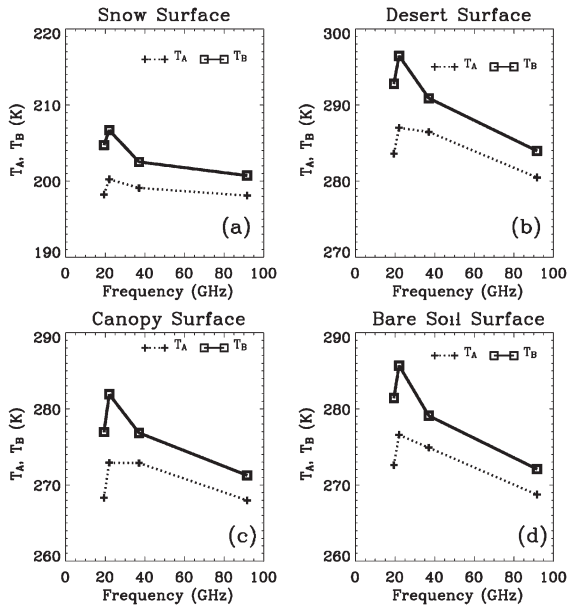

Fig. 8. Comparison of V-POL antenna temperature T_A and brightness temperature T_B spectra over four typical surfaces. (a) Snow. (b) Desert. (c) Canopy. (d) Bare soil.

spectrum. In the following emissivity and its error calculations, the antenna temperature has been converted to brightness temperatures.

For an error in the brightness temperature, i.e., ΔT_B, an error in the emissivity, i.e., $\Delta\varepsilon$, is expressed by the finite difference of (14), as follows:

$$\Delta\varepsilon = \frac{\Delta T_B}{(T_S - T_d)\zeta}. \tag{15}$$

Equation (15) shows that the error in the emissivity simulation is proportional to the error of the brightness temperature and inversely proportional to the atmospheric transmittance. At window channels, the atmospheric transmittance is usually high, and the brightness temperature associated with the downwelling radiation is small. An error of 3 K in the brightness temperature may result in an error of about 0.01 in the emissivity simulation at lower frequencies. For demonstration, Fig. 9(a) and (b) displays the global snow-free land, snow, and sea ice emissivities derived from F16 SSMIS brightness temperatures against those derived from F15 SSM/I brightness temperatures at V-POL 22.235 and 37 GHz, respectively, on January 22, 2006. Note that the emissivity from F16 SSMIS is calculated by using the SSMIS antenna temperatures with or without the remapping described in (13). Also, a time window of 1 h is used when comparing emissivities to reduce the effect of the variation of the retrieved emissivity with time. It is seen that in the presence of the errors, i.e., without the remapping using (13), the F16 emissivity at 22.235 and 37 GHz deviates from the F15 emissivity by about 0.01, which is consistent with the aforementioned analysis in (15). As the remapping technique (13) is applied to F16 SSMIS data, the so-produced F16 emissivities at all seven channels are agreeable to the corresponding F15 emissivities. Furthermore, the emissivity of global surfaces, including snow-free land, snow, and ice at two

Authorized licensed use limited to: COLORADO STATE UNIVERSITY. Downloaded on July 30,2010 at 17:20:15 UTC from IEEE Xplore. Restrictions apply.

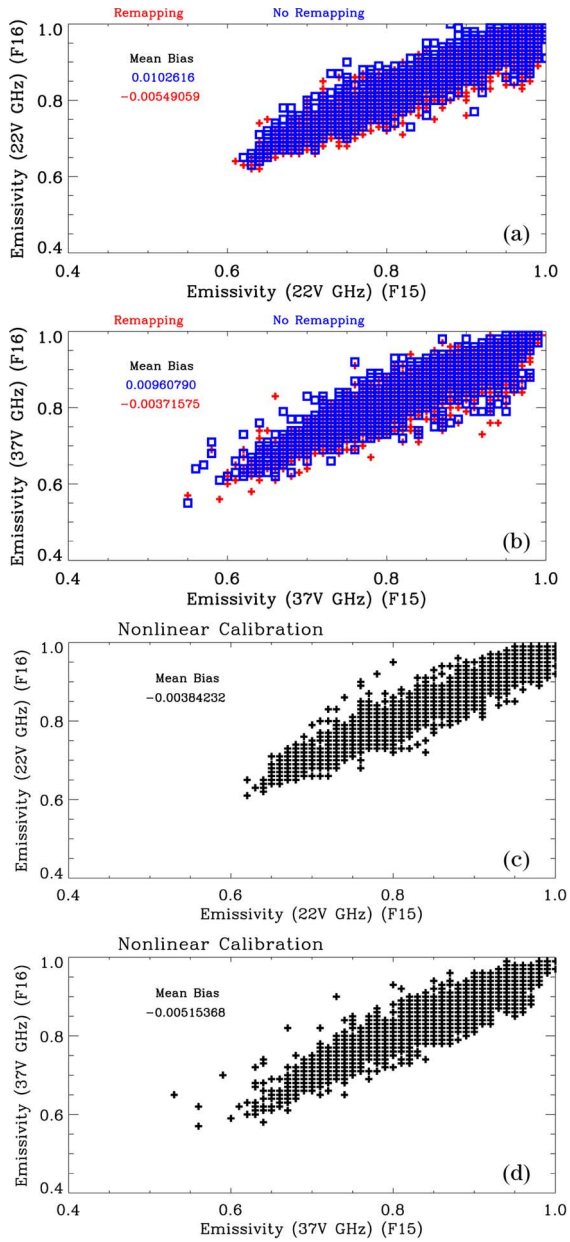

Fig. 9. Global snow-free land, snow, and sea ice emissivities derived from F16 V-POL SSMIS brightness temperatures versus the emissivity derived from F15 V-POL SSM/I brightness temperatures for 22.235 and 37 GHz on January 22, 2006, where the mean bias of emissivity between F15 and F61 is also shown. (a) 22.235 GHz. (b) 37 GHz. The F16 brightness temperatures are converted from the antenna temperatures with or without the remapping shown in Section II-C. (c) and (d) Same as (a) and (b), but the F15 and F16 data employ the nonlinear calibration using the newly derived nonlinear parameters.

frequencies, is also displayed in Fig. 9(c) and (d), respectively, which are derived from F15 and F16 brightness temperatures using the nonlinear calibration equations and newly derived nonlinear parameters. Compared to the observations without the remapping in Fig. 9(a) and (b), the F16 emissivity at two frequencies is in better agreement with the F15 emissivity. Note that the data in Fig. 9(a)–(d) cover the regions from low to high latitudes. Therefore, both the remapping coefficients and the nonlinearity parameters derived using the SCO observations at high latitudes can be very useful for improved global SSMIS imaging channel calibration.

IV. Summary and Conclusion

The SCO observations between F16 SSMIS and F15 SSM/I are utilized to assess the calibration accuracy of F16 measurements at the seven window channels from 19.35 to 91.655 GHz. For the F16 SSMIS antenna temperatures at the seven SSMI-like channels, there are biases of typically from 0.5 to 2 K with a maximum bias of more than 3 K at 22.235 GHz, with respect to F15 SSM/I. It is shown that the mean errors detected in F16 SSMIS antenna temperatures from 19.35 to 37 GHz are consistent from region to region with differences less than 0.5 K, whereas the F16 antenna temperature biases at the 91.655-GHz channels display obvious variation with the latitude and season.

The nonlinearity in F15 and F16 instruments is further investigated. Since the nonlinear parameter is not provided in SSMIS and SSM/I prelaunch analyses, a new nonlinear calibration algorithm is proposed to derive the nonlinear parameters for F15 and F16 instruments using their SCO observations. Results demonstrated that the nonlinearity is significant at some imaging channels and can reach to about 1 K at V-POL 22.235 and 37 GHz. By applying the newly derived nonlinear parameters, the SSMIS antenna temperature biases are small in comparison to F15 SSM/I nonlinear-calibrated antenna temperatures, and the derived surface emissivities between F15 and F16 are in good agreement. This demonstrates the success of the newly developed nonlinear calibration algorithm and the necessity of nonlinear calibration for conical microwave imager in the future program development.

A linear remapping is finally tested from the F16 SSMIS antenna temperature to the corresponding F15 SSM/I measurements. Note that those mapping coefficients are generated from linear calibrated F15 and F16 SCO observations because the current SSMIS and SSM/I observations utilized in the public community are calibrated from the linear calibration equation. With the so-remapped F16 antenna temperatures and suitable antenna spillover and cross-polarization corrections, the simulated emissivities at all seven channels are agreeable to the corresponding F15 emissivities. This demonstrates that the recalibrated SSMIS antenna temperatures at the seven window channels are of sufficient accuracy to be operationally used by NOAA for providing high-quality information such as the snow-free land, snow, and sea ice emissivities.

However, some improvement may be desirable in our future study. The SCO observations from SSMIS and SSM/I instruments occur only at high latitudes (relatively cold surfaces), thus limiting the dynamic range of antenna temperatures. This limitation can be mitigated using the data set covering several seasons as we did in this paper, but a better solution is to include SCO observations between F16 and Tropical Rainfall Measuring Mission Microwave Imager, which mainly occur over low latitudes. In addition, the azimuthal angle constraints should be included for finding SCO observations, particularly for microwave window channels. At window channels, microwave measurements are obtained from relatively large FOVs, and their measurements over inhomogeneous surfaces or atmospheric conditions may be dependent on the azimuthal direction. Finally, the F16 APF coefficients used in this paper could not be the best representatives of the postlaunch characterizations and may be the causes of biases between two satellites.

Authorized licensed use limited to: COLORADO STATE UNIVERSITY. Downloaded on July 30,2010 at 17:20:15 UTC from IEEE Xplore. Restrictions apply.

ACKNOWLEDGMENT

The authors would like to thank the Editor, Guest Editor, and two anonymous reviewers for their valuable suggestions that helped improve this paper.

REFERENCES

[1] G. A. Poe, K. Germain, J. Bobak, S. Swadley, J. Wessel, B. Thomas, J. Wang, and B. Burns, *DMSP Calibration/Validation Plan for the Special Sensor Microwave Imager Sounder (SSMIS)*. Washington, DC: Naval Res. Lab., 2001, ch. 1, pp. 1–32.

[2] F. Weng and N. C. Grody, "Retrieval of cloud liquid water using the Special Sensor Microwave Imager (SSM/I)," *J. Geophys. Res.*, vol. 99, no. D12, pp. 25 535–25 551, 1994.

[3] R. R. Ferraro, F. Weng, N. Grody, and A. Basist, "An eight-year (1987–1994) time series of rainfall, clouds, water vapor, snow cover, and sea ice derived from SSM/I measurements," *Bull. Amer. Meteorol. Soc.*, vol. 77, no. 5, pp. 891–905, May 1996.

[4] R. R. Ferraro, "SSM/I derived global rainfall estimates for climatological applications," *J. Geophys. Res.*, vol. 102, no. D14, pp. 16 715–16 735, 1997.

[5] B. Yan, F. Weng, and K. Okamoto, "Improved estimation of snow emissivity from 5 to 200 GHz," in *Proc. 8th Spec. Meeting Microw. Radiometry Remote Sens. Appl.*, Rome, Italy, Feb. 24–27, 2004.

[6] B. Yan and F. Weng, "A fifteen-year (1987–2002) climatology of microwave land emissivity," in *Proc. SPIE— Microwave Remote Sensing Atmosphere Environment*, Hangzhou, China, Oct. 23–27, 2002.

[7] S. Swadley, G. A. Poe, A. Uliana, and D. Kunkee, "SSMIS cal/val calibration anomaly analysis," in *Proc. NOAA-JCSDA Semin.*, Washington, DC, 2005.

[8] F. Weng, B. Yan, and N. Sun, "Correction of SSMIS radiance anomalies," in *Proc. SSMIS Work. Group Meeting*, Monterey, CA, 2005.

[9] W. Bell, S. English, and S. Swadley, "SSMIS calibration issues," in *Proc. SSMIS Work. Group Meeting*, Monterey, CA, 2005.

[10] B. Yan, F. Weng, and N. Sun, "Calibration of F16 Special Sensor Microwave Imager and Sounder (SSMIS)," in *Proc. 14th Conf. Satell. Meteorol. Oceanogr. Poster*, Atlanta, GA, 2006.

[11] D. B. Kunkee, S. D. Swadley, G. A. Poe, Y. Hong, and M. F. Werner, "Special Sensor Microwave Imager Sounder (SSMIS) radiometric calibration anomalies—Part I: Identification and characterization," *IEEE Trans. Geosci. Remote Sens.*, vol. 46, no. 4, pp. 1017–1033, Apr. 2008.

[12] S. Swadley, G. Poe, D. Kunkee, W. Bell, and Y. Hong, "Special Sensor Microwave Imager Sounder (SSMIS) radiometric calibration anomalies—Part II: Anomaly descriptions and mitigation strategies for radiance assimilation," *IEEE Trans. Geosci. Remote Sens.*, 2007, submitted for publication.

[13] W. Bell, S. J. English, B. Candy, N. Atkinson, F. Hilton, N. Baker, S. D. Swadley, W. F. Campbell, N. Bormann, G. Kelly, and M. Kazumori, "The assimilation of SSMIS radiances in numerical weather prediction models," *IEEE Trans. Geosci. Remote Sens.*, vol. 46, no. 4, pp. 884–900, Apr. 2008.

[14] B. Yan and F. Weng, "Recalibration of Special Sensor Microwave Imager and Sounder lower atmospheric sounding channels," *J. Atmos. Ocean. Technol.*, 2007. (revised). submitted for publication.

[15] C. Cao, M. Weinreb, and H. Xu, "Predicting simultaneous nadir overpasses among polar-orbiting meteorological satellites for the intersatellite calibration of radiometers," *J. Atmos. Ocean. Technol.*, vol. 21, no. 4, pp. 537–542, Apr. 2004.

[16] C. Cao, M. Goldberg, F. Weng, C. Zou, and P. Ciren, "Simultaneous nadir overpasses for NOAA-6 to NOAA-17 satellites from 1980 to 2003 for the inter-satellite calibration of radiometers," Washington, DC, NOAA Tech. Rep. NESDIS 118, 2005.

[17] C. Zou, M. Goldberg, Z. Cheng, N. Grody, J. Sullivan, C. Cao, and D. Tarpley, "Recalibration of microwave sounding unit for climate studies using simultaneous nadir overpasses," *J. Geophys. Res.*, vol. 111, no. D19, D19 114, 2006.

[18] R. A. Iacovazzi and C. Cao, "Reducing uncertainties of SNO-estimated AMSU-A relative calibration biases at surface-influenced channels," *J. Atmos. Ocean. Technol.*, 2007, to be published.

[19] B. Yan and F. Weng, "Recalibration of DMPS SSM/I for weather and climate applications," in *Proc. 15th Int. TOVS Stud. Conf.*, Maratea, Italy, Oct. 3–10, 2006.

[20] A. P. Gene, E. Uliana, B. Gardiner, and T. Rentzell, *Mitigation of DMSP F-15 RADCAL interference with SSM/I*, Nov. 2006.

[21] M. C. Colton and G. A. Poe, "Intersensor calibration of DMSP SSM/I's: F-8 to F-14, 1987–1997," *IEEE Trans. Geosci. Remote Sens.*, vol. 37, no. 1, pp. 418–439, Jan. 1999.

[22] J. P. Hollinger, J. L. Pierce, and G. A. Poe, "SSM/I instrument evaluation—Special issue on the Defense Meteorological Satellite Program (DMSP): Calibration and validation of the Special Sensor Microwave/Imager (SSM/I)," *IEEE Trans. Geosci. Remote Sens.*, vol. 28, no. 5, pp. 781–790, Sep. 1990.

[23] F. Weng, B. Yan, and N. Grody, "A microwave land emissivity model," *Geophys. Res.*, vol. 106, no. D17, pp. 20 115–20 123, 2001.

[24] S. English and T. J. Hewison, "A fast generic millimeter-wave emissivity model," in *Proc. SPIE—Microw. Remote Sens. Atmos. Environ.*, 1998, vol. 3503, pp. 288–300.

[25] T. Mo, "Prelaunch calibration of the Advanced Microwave Sounding Unit-A for NOAA-K," *IEEE Trans. Microw. Theory Tech.*, vol. 44, no. 8, pp. 1460–1469, Aug. 1996.

Banghua Yan received the Ph.D. degree in atmospheric physics from the Institute of Atmospheric Physics, Chinese Academy of Sciences, Beijing, China, in 1997 and the Ph.D. degree in atmospheric radiation from the University of Alaska, Fairbanks, in 2001.

Since November 1999, she has been with Dr. F. Weng's group in the Center for Satellite Applications and Research, National Oceanic and Atmospheric Administration (NOAA), National Environmental Satellite Data and Information Service, Camp Springs, MD. She is currently a Senior Scientist with the Joint Center for Satellite Data Assimilation (JCSDA), NOAA. She is also with Perot, Inc., Camp Springs, MD. In the past few years, she has directly contributed in the development of microwave land, snow, and sea ice emissivity models, which have significantly improved the use of satellite sounding data in numerical weather prediction (NWP) models and impacted the high-latitude weather forecasts. These land, snow, and sea ice microwave emissivity models have been implemented into the NOAA National Centers for Environmental Prediction NWP model and the JCSDA community radiative transfer model, which has been successfully used in several operational data assimilation systems in the U.S. She has authored or coauthored more than ten papers published in international journals and conference proceedings. Her current research interests include the following: 1) land and snow microwave emissivity modeling and retrievals; 2) DMPS SSM/I and SSMIS satellite sensor calibration; 3) assimilation impacts of microwave satellite measurements on global NWP models; and 4) ocean color remote sensing.

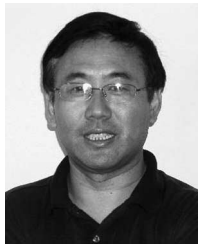

Fuzhong Weng received the Ph.D. degree from Colorado State University, Fort Collins, in 1992.

He is the Chief of the Sensor Physics Branch, Center for Satellite Applications and Research, National Oceanic and Atmospheric Administration (NOAA), National Environmental Satellite Data and Information Service, Camp Springs, MD. In the past years, he has been leading the development of NOAA operational satellite microwave products and algorithms from the Special Sensor Microwave Imager and Advanced Microwave Sounding Unit. He is the National Polar Environmental Satellite Systems (NPOESS) microwave operational algorithm team member. He is a science lead in developing the community radiative transfer model, which has been successfully used in several operational data assimilation systems in the U.S. He has also directly contributed in the development of microwave land, snow, and sea ice emissivity models, which have significantly improved the use of satellite sounding data in numerical weather prediction (NWP) models and impacted the high-latitude weather forecasts. He is currently developing new innovative techniques to advance the use of satellite measurements under cloudy and precipitation areas in NWP models. He has authored or coauthored more than 70 papers published in international journals and conference proceedings.

Dr. Weng was the recipient of various awards, which include the following: the David Johnson Award in 2000 for his outstanding contributions to satellite microwave remote sensing fields and the utilization of satellite data in the NWP models from NOAA; the Scientific Achievement Award in 2002 for excellence in developing operational satellite microwave products and algorithms from the International Society for Optical Engineers (SPIE); the Bronze Medal Award in 2004 for developing operational microwave products to improve weather and climate predictions and the Gold Medal Award in 2005 for his achievements in satellite data assimilation, both from the U.S. Department of Commerce; and the Bronze Medal Award for leading the successful NOAA-18 instrument calibration from NOAA.

Authorized licensed use limited to: COLORADO STATE UNIVERSITY. Downloaded on July 30,2010 at 17:20:15 UTC from IEEE Xplore. Restrictions apply.